

Birchite, a new mineral from Broken Hill, New South Wales, Australia: Description and structure refinement

PETER ELLIOTT,^{1,*} JOËL BRUGGER,^{1,2} ALLAN PRING,² MARCUS L. COLE,^{3,†} ANTHONY C. WILLIS,⁴ AND UWE KOLITSCH⁵

¹School of Earth and Environmental Sciences, University of Adelaide, Adelaide, South Australia 5005, Australia

²South Australian Museum, North Terrace, Adelaide, South Australia 5000, Australia

³School of Chemistry and Physics, University of Adelaide, Adelaide, South Australia 5005, Australia

⁴Research School of Chemistry, Australian National University, Australian Capital Territory 0200, Australia

⁵Mineralogisch-Petrographische Abt., Naturhistorisches Museum, A-1010 Wien, Austria

ABSTRACT

The new mineral species birchite, idealized formula $\text{Cd}_2\text{Cu}_2(\text{PO}_4)_2(\text{SO}_4)\cdot 5\text{H}_2\text{O}$, occurs on specimens from the Block 14 Opencut, Broken Hill, New South Wales, Australia, as sprays and aggregates of crystals to 0.75 mm across on a host rock composed of quartz, garnet, galena, chalcopyrite, and fluorapatite. It is a late-stage supergene mineral formed as part of a suite of secondary phosphate minerals under low-temperature conditions. Associated secondary minerals are covellite, cerussite, anglesite, plumbogummite-hinsdalite, pyromorphite, libethenite, and sampleite. Individual crystals are bladed to prismatic and acicular in habit, with a maximum length of 0.3 mm and width of 0.05 mm. The crystals are elongated along [001] and sometimes also flattened on (100). The crystal forms are major {100} and {010}, and minor {101} and {001}. Birchite is orthorhombic, space group *Pnma*, with unit-cell parameters refined from powder X-ray diffraction data, $a = 10.489(6)$, $b = 20.901(7)$, $c = 6.155(5)$ Å, $V = 1349.6(3)$ Å³, and $Z = 4$. The eight strongest lines in the diffraction pattern are [$d(\text{Å})/I(hkl)$]: 10.451(100)(020); 5.146(28)(111); 4.223(38)(131); 3.484(39)(060); 2.902(70)(260); 2.719(33)(132); 2.652(32)(042); 1.919(80)(432). Birchite is translucent (masses) to transparent (crystals); pale blue with a vitreous luster. Optically, birchite is biaxial positive, with $n_\alpha = 1.624(4)$, $n_\beta = 1.636(5)$, $n_\gamma = 1.669(4)$, and $2V_{\text{calc}} = +63^\circ$. The optical orientation is $\mathbf{X} = \mathbf{b}$, $\mathbf{Y} = \mathbf{a}$, $\mathbf{Z} = \mathbf{c}$; the optical axis plane lies within the {100} plane. Birchite shows very faint pleochroism, $\mathbf{X} =$ pale bluish, $\mathbf{Z} =$ pale greenish, absorption $\mathbf{Z} \geq \mathbf{X}$. Birchite is brittle, has a conchoidal fracture and is nonfluorescent. Hardness (Mohs) is 3.5–4; the measured density is 3.61(4) g/cm³, and the calculated density is 3.647 g/cm³ (from the empirical formula). Average electron microprobe analysis (wt%): CdO 36.79, CuO 21.22, CaO 0.17, MnO 0.17, ZnO 1.07, P₂O₅ 20.21, SO₃ 9.70, H₂O (from crystal-structure analysis) 12.37, total 101.70. The empirical formula, calculated on the basis of 17 O atoms and with H₂O calculated to give 5H₂O is $(\text{Cu}_{1.94}\text{Zn}_{0.10})_{\Sigma 2.04}(\text{Cd}_{2.09}\text{Ca}_{0.02}\text{Mn}_{0.02})_{\Sigma 2.13}\text{P}_{2.07}\text{S}_{0.88}\text{O}_{12}\cdot 5\text{H}_2\text{O}$. The crystal structure has been refined to an *R* index of 4.3% for 846 observed reflections measured with MoK α X-radiation. Alternating [CdO₄(H₂O)₂] octahedra and [CuO₃(H₂O)₂] square-pyramids share edges to form chains that extend along the *a* axis, which are linked by (PO₄) tetrahedra to form [CdCu(PO₄)(H₂O)₂O] sheets in the (010) plane. Two such sheets are linked via (PO₄) tetrahedra vertices to form a layer in the (010) plane. Two layers, which are related by mirror symmetry, are linked via (SO₄) tetrahedra vertices to form a heteropolyhedral framework structure. Interstitial channels within the framework extend along both the *a* and *c* axes and are occupied by a H₂O group. The mineral is named for William D. Birch, Senior Curator of Geosciences at Museum Victoria, Australia.

Keywords: Birchite, new mineral species, crystal structure, cadmium oxysalt, phosphate, sulfate, Broken Hill, New South Wales

INTRODUCTION

In a detailed description of the mineralogy of the Broken Hill Ag, Pb, Zn deposit, New South Wales, Australia, Birch (1999) reported several unknown minerals, including a cadmium-copper phosphate. This mineral has now been characterized in detail and

is the subject of this paper. It is the second known Cd-bearing phosphate mineral, after goldquarryite (Roberts et al. 2003), and it is only the fourteenth mineral to contain essential cadmium (Cooper et al. 2000).

The mineral is named for William D. Birch, Senior Curator of Geosciences at Museum Victoria, Australia, in recognition of his contribution to Australian geological sciences, and also his service to several professional organizations. The mineral and its name have been approved by the IMA Commission on New

* E-mail: peter.elliott@adelaide.edu.au

† Current address: School of Chemistry, University of New South Wales, Sydney 2052, Australia.

Minerals, Nomenclature and Classification (IMA 2006-048). Type material is preserved in the Department of Mineralogy of the South Australian Museum, Adelaide, South Australia (Registration number G30968).

OCCURRENCE AND ASSOCIATED MINERALS

The Broken Hill deposit, situated in western New South Wales, has been mined continuously since 1883, when the first lease was pegged by boundary rider Charles Rasp. It is Australia's largest base metal deposit and most mineralogically diverse mineral deposit, with almost 300 mineral species recorded, including 10 minerals new to science (Birch et al. 1982; Birch 1999).

The origin of the deposit has long been controversial, but it is now generally considered to be an intensely deformed and metamorphosed stratiform deposit of submarine exhalative origin (Stanton 1976; Plimer 1984). The ore body occurs in an early Proterozoic sequence of gneisses, amphibolites, migmatites, and "lode horizon" rocks that were deposited as marine sediments and volcanics 1820 million years ago (Plimer 1984). These were subjected to prograde metamorphism up to granulite facies, with two phases of metamorphism, during the Olarian Orogeny at 1660 Ma. During a later phase of retrograde metamorphism and deformation, major shear zones developed along large faults, which folded and remobilized the orebody.

Primary sulfides are rich in Pb, Zn, Ag, Mn, and Cu, with significant amounts of F, P, As, Sb, Co, Ni, and Cd. The orebody was capped by a massive coronadite-quartz gossan, below which an oxidized zone formed at the top of the central arch of the ore lenses, and extended to an average depth of 75 m. The oxidized zone has had a long and complex history, which is reflected in the complexity of its mineralogy.

Mining of remnant sulfide and oxidized ore in the Blackwood, Kintore and Block 14 Opencuts by Minerals, Mining, and Metallurgy Limited commenced in 1972 and continued until 1992. An extensive suite of secondary minerals was exposed, including oxides, carbonates, sulfates, phosphates, arsenates, halides, silicates, and native metals. As a result of these mining operations the number of mineral species recorded from Broken Hill increased by ~70 (Birch and van der Heyden 1988, 1997; Birch 1990). The new species mawbyite, kintoreite, and segnitite were described from specimens collected during this time (Pring et al. 1989, 1995; Birch et al. 1992).

During the late 1990s, a small-scale mining operation recovered oxidized ore from the Kintore and Block 14 Opencuts, which was transported to the Pinnacles Mine, 15 km southwest of Broken Hill, for processing. Birchite occurs on specimens collected from these stockpiles in 1998. The exact area of the Block 14 Opencut, which was the source of the specimens is unknown, however, the assemblage of phosphate minerals on the specimens suggests they may be from the No. 3 Lens between the 290 and 275 m levels (Birch and van der Heyden 1997).

Birchite occurs in small cavities and thin seams in a quartz-garnet matrix throughout which are disseminated abundant small, corroded masses of galena and fluorapatite, plus minor chalcopyrite and covellite. Crusts of pale yellow hinsdalite-plumbogummite line cavities and seams. Associated minerals are small colorless cerussite and anglesite crystals and masses, prisms of white pyromorphite, sprays of pale green libethenite

prisms and hemispheres of platy, royal blue sampleite crystals. The sampleite contains significant concentrations of Cd and Pb, and some crystals have a composition that may represent the Pb-dominant analog. Plumboan and cadmian-plumboan sampleite and calcian, calcian-phosphatian, and cadmian zdenekite from Broken Hill have previously been noted (Birch and van der Heyden 1997; Birch 1999; Giester et al. 2007).

Birchite is a late-stage supergene mineral formed under low-temperature conditions as part of a suite of secondary phosphate minerals. The following paragenesis for the suite of phosphates from the Block 14 Opencut has been proposed by Birch and van der Heyden (1997):

corkite-hinsdalite → tsumebite → pyromorphite → scholzite → libethenite → kintoreite → sampleite/beraunite/strengite → torbernite.

The overall sequence of crystallization likely represents a change from acid to more alkaline conditions (Nriagu 1984; Williams 1990).

The Cd-bearing secondary minerals otavite, CdCO_3 , gold-quarryite, $\text{CuCd}_2\text{Al}_3(\text{PO}_4)_4\text{F}_2(\text{H}_2\text{O})_{10}(\text{H}_2\text{O})_2$, and niedermayrite, $\text{Cu}_2\text{Cd}(\text{SO}_4)_2(\text{OH})_6 \cdot 4\text{H}_2\text{O}$, occur in the Broken Hill oxidized zone and several arsenates (conichalcite-duftite, lavendulan, and zdenekite), phosphates (sampleite), and sulfates (serpierite) contain, sometimes significant, cadmium replacing lead and calcium (P. Elliott, unpublished data 2006).

Sphalerite in the Broken Hill ore body contains small concentrations of cadmium (Edwards 1955) and the cadmium sulfides greenockite and hawleyite both occur in the oxidized zone (Birch 1999). One or more of these is most likely the source of the cadmium in the secondary minerals.

APPEARANCE, PHYSICAL, AND OPTICAL PROPERTIES

Birchite occurs as sprays and aggregates of radiating crystals, which reach a maximum 0.75 mm across, but are more typically less than 0.5 mm across. Individual crystals are bladed (more or less lath-shaped) and prismatic to acicular in habit and reach a maximum of approximately 0.3 mm in length and 0.05 mm in width (Figs. 1 and 2). Crystals are elongated along [001] and sometimes also flattened on (100) (Fig. 3). The dominant crystal forms observed are {100} and {010}. The majority of crystals show no termination faces, but those that do have minor {101}, and sometimes also {001} faces. No twinning has been observed. The mineral is brittle with a conchoidal fracture. Birchite is translucent (masses) to transparent (crystals) and the color is pale blue (No. 106C on the Royal Horticultural Society, London color chart). The streak is white and the luster vitreous. The Mohs hardness is 3.5–4. The measured density, by suspension in a mixture of Clerici solution and water, is $3.61(4) \text{ g/cm}^3$, and the calculated density is 3.647 g/cm^3 , based on the empirical chemical formula with $Z = 4$, and 3.583 g/cm^3 based on the simplified formula derived from the structure refinement.

Optically, birchite is biaxial positive, with $n_\alpha = 1.624(4)$, $n_\beta = 1.636(5)$, $n_\gamma = 1.669(4)$, and (values obtained in white light using Cargille immersion liquids), and $2V_{\text{calc}} = +63^\circ$. Some crystals show a small variability for the refractive index γ : the top area of the lath gives a somewhat lower value than the remainder; the

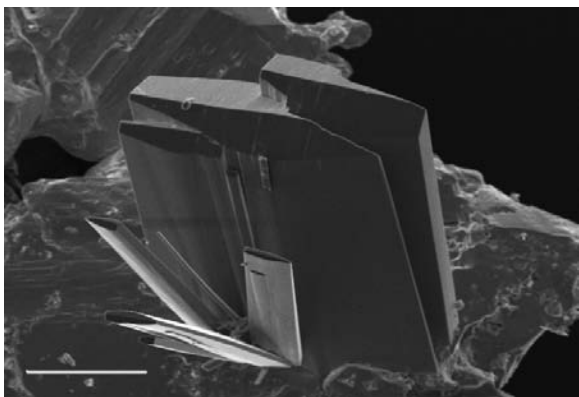


FIGURE 1. SEM photomicrograph showing bladed crystals of birchite on anglesite. The crystals are flattened on (100) and show the principal forms {100}, {010}, and {101}. The scale bar is 50 μm long.

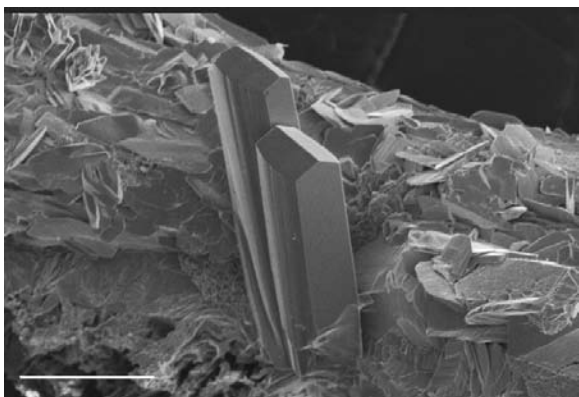


FIGURE 2. SEM photomicrograph showing prismatic crystals of birchite on anglesite. The crystals are elongated along [001] and show the crystal forms {100}, {010}, and {101}. The scale bar is 50 μm long.

standard uncertainties given were increased to reflect this small variability (probably caused by some substitutions involving the divalent metals). The optical orientation is $\mathbf{X} = \mathbf{b}$, $\mathbf{Y} = \mathbf{a}$, $\mathbf{Z} = \mathbf{c}$, i.e., the optical elongation of the lath-shaped crystals is invariably positive. A value for $2V$ could not be measured since the optical axis plane lies within the plane of the tabular form {100}. Birchite shows very faint pleochroism, $\mathbf{X} =$ pale bluish, $\mathbf{Z} =$ pale greenish, absorption $\mathbf{Z} \geq \mathbf{X}$. Judging from the interference colors, the minerals shows no or only very small dispersion.

CHEMICAL COMPOSITION

Several grains of the mineral were embedded in epoxy resin, polished, and carbon coated. Birchite was analyzed with a CAMECA SX51 electron microprobe operating in the wavelength-dispersion mode, with an accelerating voltage of 15 kV, a specimen current of 10 nA, and a beam diameter of 20 μm . The mineral was very unstable under the electron beam, suggesting that water and possibly other components were being driven off, which has resulted in some deviation from the theoretical stoichiometry. To minimize beam damage the beam was defocused to 20 μm , and the mineral was analyzed with micromovement of a homogenous grain under the electron beam several times during the counting period. The standards employed were cadmium metal (CdL α), chalcocopyrite (CuK α), sphalerite (ZnK α), hydroxylapatite (CaK α and PK α), galena (PbM α and SK α), and rhodnite (MnK α). Analytical results are given in Table 1. The elements Al, Si, As, F, and Cl were detected only in trace amounts (<0.05 wt%) and the elements Na, K, Fe, and V were sought but not detected. The absence of K and Na was determined following

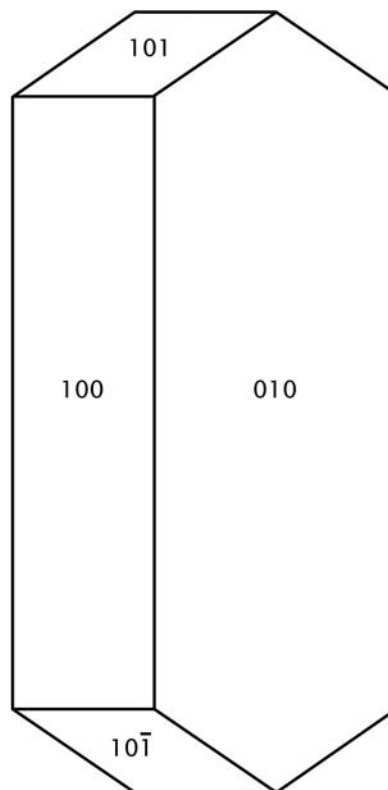


FIGURE 3. Crystal drawing showing a prismatic crystal of birchite, elongated parallel to [001]. Crystal modeled with SHAPE V7.1.2 (Shape Software 2004).

TABLE 1. Compositional data for the birchite

Constituent	wt%	Range	Standard deviation
CuO	21.22	19.68–22.78	1.04
ZnO	1.07	0.11–1.70	0.37
CaO	0.17	0.14–0.26	0.04
MnO	0.17	0.11–0.29	0.05
PbO	0.07	0.00–0.25	0.10
CdO	36.79	34.10–38.79	1.80
P ₂ O ₅	20.21	16.47–21.79	1.32
SO ₃	9.70	8.62–10.71	0.70
H ₂ O*	12.37		
Total	101.77		

Note: Number of analyses = 13.

* Calculated from structure determination. The empirical formula based on 17 oxygen atoms is $(\text{Cu}_{1.94}\text{Zn}_{0.10})_{\Sigma 2.04}(\text{Cd}_{2.09}\text{Ca}_{0.02}\text{Mn}_{0.02})_{\Sigma 2.13}\text{P}_{2.07}\text{S}_{0.88}\text{O}_{12} \cdot 5\text{H}_2\text{O}$, and the idealized formula, confirmed by structure analysis, is $\text{Cd}_2\text{Cu}_2(\text{PO}_4)_2(\text{SO}_4) \cdot 5\text{H}_2\text{O}$.

correction for potential CdL β /K $K\alpha$ and ZnL β /NaK α overlaps, respectively. An energy-dispersion scan showed the absence of any elements with atomic number greater than 9 except those reported. The valence states of Cu and Cd and the number of O atoms were determined by crystal-structure analysis prior to final interpretation of the electron-microprobe results. The Cameca PAP $\phi(\rho Z)$ matrix correction procedure was used in data reduction (Pouchou and Pichoir 1985). The average of 13 spot analyses gave (wt%): CdO 36.79, CuO 21.22, CaO 0.17, MnO 0.17, ZnO 1.07, P₂O₅ 20.21, SO₃ 9.70, and H₂O 12.37 (calculated from structure determination). The empirical formula, based 12 anhydrous O atoms, is $(\text{Cu}_{1.94}\text{Zn}_{0.10})_{\Sigma 2.04}(\text{Cd}_{2.09}\text{Ca}_{0.02}\text{Mn}_{0.02})_{\Sigma 2.13}\text{P}_{2.07}\text{S}_{0.88}\text{O}_{12} \cdot 5\text{H}_2\text{O}$, and the idealized formula, confirmed by structure analysis, is $\text{Cd}_2\text{Cu}_2(\text{PO}_4)_2(\text{SO}_4) \cdot 5\text{H}_2\text{O}$.

Due to the limited amount of material available, a quantitative determination of H₂O was not carried out. H₂O was however confirmed from the crystal structure analysis. The Gladstone-Dale compatibility index is –0.017, indicating “superior” agreement between the chemical and physical data (Mandarino 1981). Birchite is slowly soluble, without effervescence, in cold 10% HCl.

Powder X-ray diffraction data

Powder X-ray diffraction data (Table 2) were obtained using a 100 mm Guinier-Hägg camera using $\text{CrK}\alpha$ radiation ($\lambda = 2.28970 \text{ \AA}$) and silicon (NBS SRM 640a) as an internal standard. The Guinier-Hägg film was scanned using an Epson film scanner, and the powder-diffraction profile over the 2θ range 10 to 80° was extracted using the program SCION IMAGE and the Universal-Si-Calibration, a macro function based on IGOR PRO 4.0 (WaveMetrics, Inc. 2000). The unit-cell parameters were refined by treating the whole powder pattern with the Le Bail profile-fitting method (Le Bail et al. 1988), starting from the unit-cell parameters determined from single-crystal techniques. The final unit-cell parameters, $a = 10.489(6)$, $b = 20.901(7)$, $c = 6.155(5) \text{ \AA}$, and $V = 1349.6(3) \text{ \AA}^3$, are very similar to those obtained from the single-crystal refinement. The axial ratios calculated from these cell parameters are 3.3958:1:1.7041. Indexing of the powder pattern was based on intensities calculated from the structure refinement (Yvon et al. 1977).

Single-crystal X-ray diffraction

Single-crystal intensity data, using a crystal with approximate dimensions of $0.08 \times 0.02 \times 0.02 \text{ mm}$, were collected on Nonius KappaCCD diffractometer (MoK α radiation) at 293 K. A total of 10753 reflections were collected from $\theta = 3.5\text{--}25.0^\circ$, of which 1227 were unique, with 846 classified as observed, ($|F_o| > 4\sigma(F_o)$). The measured intensities were corrected for Lorentz and polarization effects and a Gaussian integration absorption correction, based on the crystal size and indexing of faces, was applied (Coppens 1970). The resulting minimum and maximum transmission factors were 0.608 and 0.837. Data reduction and cell refinement were carried out using the Denzo and Scalepack and HKL Scalepack programs (Otwinowski et al. 2003). Conditions for the data collection and subsequent refinement are summarized in Table 3.

Structure solution and refinement

The crystal structure was solved in space group $Pnma$ by Patterson methods (SHELXS-97, Sheldrick 1997a) and subsequent Fourier and difference Fourier synthesis. Final structure parameters were obtained by full-matrix least squares techniques on F^2 (SHELXL-97, Sheldrick 1997b). Complex scattering factors for neutral atoms were taken from the *International Tables for Crystallography* (Wilson 1992). Refinement of all atom-position parameters, allowing for anisotropic displacement of non-H atoms and the inclusion of a weighting scheme of

the structure factors, resulted in a final agreement index ($R1$) of 4.30%, for 846 observed reflections and a total of 116 refined parameters. Final positional and displacement parameters are given in Table 4. Selected interatomic distances and angles are given in Table 5. No H atoms were detected in the difference Fourier map and the concept of bond-valences (Bresle and O'Keeffe 1991) was used to identify the water molecules (Table 6).

CRYSTAL STRUCTURE DESCRIPTION

Cation sites

The structure of birchite contains one Cu site, occupied by Cu with minor Zn, with each Cu^{2+} cation coordinated by three O atoms, and two (H_2O) groups (Fig. 4). The geometry of the arrangement is closer to that of a distorted square-pyramid rather than a trigonal-pyramid (Effenberger 1988), with a O5-Cu-O7 angle of 161.4° (ideal: square-pyramid; 180° ; trigonal-pyramid; 120°), and a O5-Cu-H₂O2 angle of 93.7° (ideal: square-pyramid; 90° ; trigonal-pyramid; 180°) (Table 5). The square-pyramid has four equatorial Cu- ϕ (ϕ : O²⁻, H₂O) bond lengths of 1.913, 1.923, 1.969, and 2.056 \AA , and one apical ligand at 2.359 \AA (Table 5). The variation in both individual and $\langle \text{Cu}-\phi \rangle$ (ϕ : unspecified ligand) distances are within the range (1.880–2.519 \AA) of those compiled by Eby and Hawthorne (1990) and Burns and Hawthorne (1995) for fivefold-coordinated Cu^{2+} in minerals, although the deviation from equal bond lengths in the ($\text{Cu}\phi_5$) polyhedron is larger than is normal in such polyhedra in minerals. The square-pyramidal geometries show significant elongation to the apical (H₂O2), in addition to large angular deviation between the apical and equatorial oxygen atoms (Fig. 4, Table 5). Polyhedron geometry and bond-valence sums (Table 6) demonstrate that Cu is present as Cu^{2+} .

Cu^{2+} occurs in several coordination polyhedra in oxysalt minerals (square-planar, trigonal-bipyramidal, square-pyramidal,

TABLE 2. X-ray powder diffraction data for birchite

l_{obs}	d_{obs}	l_{calc}	d_{calc}	h	k	l	l_{obs}	d_{obs}	l_{calc}	d_{calc}	h	k	l
100	10.451	100	10.447	0	2	0	20	2.480	6	2.482	2	3	2
15	5.905	3	5.912	0	1	1	5	2.456	1	2.458	3	5	1
25	5.309	14	5.313	1	0	1	5	2.331	1	2.337	2	8	0
5	5.245	3	5.239	2	0	0			2	2.311	3	0	2
10	5.226	9	5.224	0	4	0	5	2.306	1	2.308	0	6	2
30	5.146	12	5.149	1	1	1	10	2.291	1	2.290	3	6	1
5	5.087	3	5.081	2	1	0	5	2.251	1	2.254	1	6	2
5	4.733	1	4.736	1	2	1	5	2.221	1	2.219	4	5	0
5	4.688	1	4.683	2	2	0	5	2.191	1	2.193	3	3	2
5	4.613	1	4.616	0	3	1	5	2.174	1	2.173	0	9	1
40	4.223	14	4.224	1	3	1	10	2.130	6	2.129	3	7	1
15	3.992	4	3.992	2	0	1			1	2.127	1	9	1
20	3.724	9	3.725	1	4	1	5	2.128	1	2.123	2	9	0
		2	3.699	2	4	0	10	2.107	1	2.112	2	6	2
40	3.484	13	3.482	0	6	0	5	2.095	4	2.093	4	6	0
5	3.464	2	3.463	2	3	1	10	2.013	3	2.016	1	0	3
15	3.269	10	3.267	2	5	0	5	2.003	1	2.007	1	1	3
10	3.078	3	3.082	0	2	5	5	1.982	1	1.975	5	1	1
10	3.009	6	3.007	3	1	1	10	1.955	2	1.957	1	8	2
10	2.953	2	2.957	1	0	2	10	1.945	6	1.944	1	10	1
20	2.924	6	2.928	1	1	2	80	1.919	2	1.919	4	3	2
15	2.913	2	2.912	1	6	1	10	1.911	3	1.913	2	0	3
70	2.902	2	2.900	2	6	0			1	1.905	2	1	3
20	2.842	4	2.845	1	2	2	15	1.879	1	1.882	2	2	3
25	2.787	14	2.785	3	3	1	5	1.865	2	1.864	4	4	2
30	2.719	8	2.722	1	3	2	5	1.843	1	1.845	2	3	3
30	2.652	5	2.654	0	4	2	5	1.824	1	1.826	1	9	2
5	2.625	5	2.624	2	6	1	5	1.814	1	1.816	1	5	3
10	2.622	5	2.619	4	0	0	10	1.804	3	1.801	4	5	2
5	2.613	1	2.612	0	8	0	10	1.795	1	1.796	2	4	3
25	2.595	2	2.599	2	7	0	5	1.787	1	1.789	1	11	1
10	2.544	4	2.541	4	2	0	10	1.787	3	1.786	2	11	0

Note: Intensities estimated visually.

TABLE 3. Crystal data, data collection, and refinement details

Crystal data	
Formula	$\text{Cd}_2\text{Cu}_2(\text{PO}_4)_2(\text{SO}_4)\cdot 5\text{H}_2\text{O}$
Formula weight	728.00
Space group	$Pnma$
a, b, c (\AA)	10.4768(8), 20.8938(14), 6.1640(3)
V (\AA^3), Z	1349.3(3), 4
D (calc) (g/cm^3)	3.647
$F(000)$	1037.9
μ (mm^{-1})	5.03
Absorption correction	Gaussian integration
Crystal dimensions (mm)	$0.08 \times 0.02 \times 0.02$
Data collection	
Diffractometer	Nonius KappaCCD
Temperature (K)	293
Radiation	MoK α , $\lambda = 0.71073 \text{ \AA}$
Crystal detector distance	28 mm
Rotation axis, width ($^\circ$)	$\omega, 1.5$
Total number of frames	169
Collection time per degree ($^\circ$)	600
θ range ($^\circ$)	3.5–25.0
h, k, l ranges	$-7 \rightarrow 6, -12 \rightarrow 11, -24 \rightarrow 24$
Total reflections measured	10753
Unique reflections	1227 ($R_{\text{int}} = 1.72\%$)
Refinement	
Refinement on	F^2
$R1^*$ for $F_o > 4\sigma(F_o)$	4.30%
$wR2^*$ for all F_o^2	10.80%
Reflections used $F_o^2 > 4\sigma(F_o^2)$	846
Number of parameters refined	116
GoF	1.044

* $R1 = \sum ||F_o| - |F_c|| / \sum |F_o|$.

† $wR2 = \sum w(|F_o|^2 - |F_c|^2)^2 / \sum w|F_o|^2$; $w = 1/[\sigma^2(F_o^2) + (0.042P)^2 + 12.60P]$; $P = ([\text{max}(0 \text{ or } F_o^2)] + 2F_c^2)/3$.

TABLE 4. Fractional coordinates and displacement parameters (\AA^2) for atoms for birchite

	<i>x</i>	<i>y</i>	<i>z</i>	U_{eq}	U_{11}	U_{22}	U_{33}	U_{12}	U_{13}	U_{23}
Cd	0.90709(8)	0.60270(4)	0.54392(13)	0.0237(3)	0.0252(5)	0.0243(4)	0.0216(4)	-0.0024(4)	0.0028(4)	-0.0007(4)
Cu	0.10856(13)	0.56327(6)	0.12074(19)	0.0192(3)	0.0231(8)	0.0232(7)	0.0113(6)	-0.0005(5)	-0.0001(6)	0.0042(6)
P	0.1735(3)	0.54334(12)	0.6333(4)	0.0163(6)	0.0201(16)	0.0177(13)	0.0111(12)	-0.0012(11)	0.0002(12)	0.0014(11)
S	0.9468(4)	0.75	0.7596(7)	0.0239(9)	0.027(2)	0.0210(19)	0.024(2)	0	0.0003(17)	0
O1	0.9880(11)	0.75	0.9852(17)	0.034(3)	0.029(7)	0.044(7)	0.028(7)	0	-0.017(5)	0
O2	0.8066(11)	0.75	0.7490(15)	0.024(3)	0.029(7)	0.026(6)	0.017(5)	0	-0.004(5)	0
O3	0.9999(8)	0.6926(4)	0.6491(13)	0.038(2)	0.031(6)	0.033(5)	0.052(5)	-0.015(4)	0.010(4)	0.002(4)
O4	0.2888(7)	0.5865(3)	0.6574(11)	0.0202(17)	0.022(4)	0.019(4)	0.020(4)	-0.008(3)	0.001(3)	-0.004(3)
O5	0.0764(7)	0.5489(3)	0.8175(10)	0.0196(17)	0.016(4)	0.032(4)	0.010(4)	-0.008(3)	0.002(3)	0.004(3)
O6	0.2181(7)	0.4729(3)	0.6099(10)	0.0191(16)	0.022(4)	0.018(4)	0.017(4)	-0.003(3)	0.000(3)	0.008(3)
O7	0.0925(7)	0.5617(3)	0.4298(10)	0.0192(16)	0.022(4)	0.027(4)	0.009(3)	0.003(3)	-0.004(3)	0.004(3)
H ₂ O1	0.9503(7)	0.6211(3)	0.1418(11)	0.0218(17)	0.031(5)	0.019(4)	0.015(3)	-0.003(3)	-0.004(3)	0.004(3)
H ₂ O2	0.2212(7)	0.6593(3)	0.0593(11)	0.0211(17)	0.017(4)	0.020(4)	0.026(4)	0.007(3)	-0.001(3)	0.001(3)
H ₂ O3	0.6947(11)	0.75	0.1385(16)	0.030(3)	0.028(7)	0.040(7)	0.023(6)	0	0.001(5)	0

Note: The anisotropic displacement factors (U_{ij}) are defined as $\exp[-2\pi^2 \sum_{i,j=1}^3 h_i U_{ij} a_j^* \mathbf{a}_i^* \mathbf{h}_j]$.

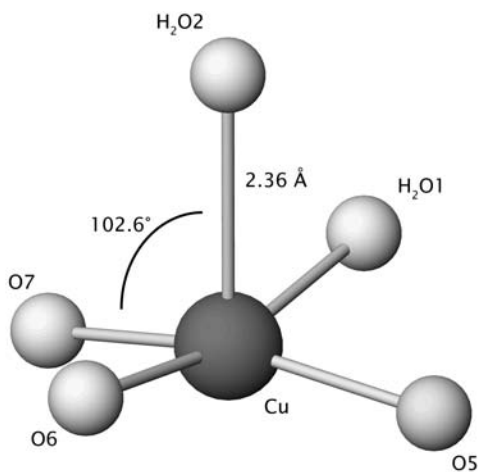


FIGURE 4. Coordination of the Cu site in birchite. All structure drawings were completed using ATOMS (Shape Software 1997).

and octahedral) and the geometries are frequently significantly distorted from the ideal (Burns and Hawthorne 1995). Distorted geometries can be considered as intermediate between the different regular geometries, and may define structural pathways between the different coordination polyhedra.

The structure contains one Cd site occupied by Cd with minor Ca and Mn, and coordinated by four O atoms and two *cis* (H₂O) groups in a distorted octahedral arrangement (Table 5; Fig. 5). As shown in Figure 5, there is also an additional quite short Cd-O5 approach of 2.692 Å, a similar situation to that in the structure of keyite (Cooper and Hawthorne 1996). The bond-valence sum incident at the Cd atom is satisfied from the nearest six anions (Table 6) without the contribution from O5, hence the interaction is not considered significant. The distorted octahedra have a <Cd-O, (H₂O)> bond distance of 2.311 Å [range: 2.211–2.549 Å], which compares well with the average of 2.305 Å [range: 2.169–2.446 Å] for Cd²⁺ in octahedral coordination in other cadmium oxysalt minerals (Cooper and Hawthorne 1996, 2000, 2004; Giester et al. 1998). Coordination of Cd²⁺ in oxysalt minerals is exclusively octahedral.

The O6-Cd-H₂O1, O7-Cd-H₂O1, H₂O2-Cd-H₂O1, H₂O2-Cd-O6, and O7-Cd-O4 angles (78.5, 66.3, 79.0, 76.1, and 132.8°, respectively) depart from the ideal value of 90° for a holosymmetric octahedron, which is due to linkage of the polyhedra.

TABLE 5. Selected interatomic distances (Å), angles (°), and suggested hydrogen bonds for birchite

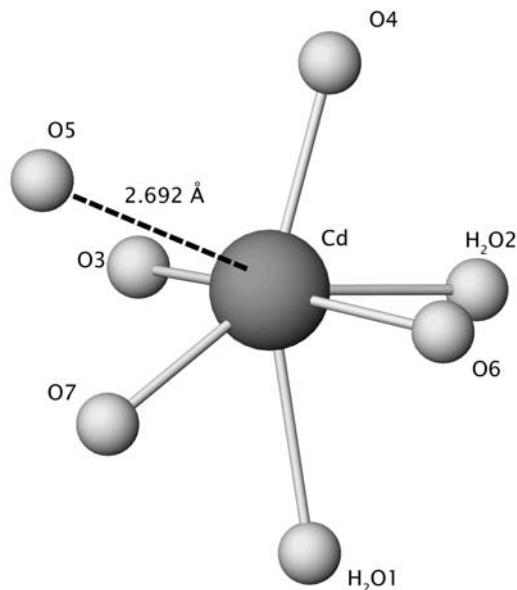
Cd-O3	2.211(8)	P-O4	1.515(8)
Cd-O7	2.237(7)	P-O5	1.529(7)
Cd-O6	2.245(7)	P-O6	1.550(7)
Cd-O4	2.262(7)	P-O7	1.562(7)
Cd-H ₂ O1	2.365(7)	<P-O>	1.539
Cd-H ₂ O2	2.549(7)		
<Cd-O>	2.312		
Cu-O7	1.913(6)	S-O1	1.456(11)
Cu-O5	1.923(6)	S-O2	1.470(12)
Cu-O6	1.969(7)	S-O3 ×2	1.488(8)
Cu-H ₂ O1	2.056(7)	<S-O>	1.476
Cu-H ₂ O2	2.359(7)		
<Cu-O>	2.044		
O3-Cd-O7	92.0(3)	O7-Cu-O5	161.9(3)
O3-Cd-O4	97.4(3)	O7-Cu-O6	96.2(3)
O7-Cd-O4	132.8(3)	O5-Cu-O6	94.0(3)
O3-Cd-O6	166.2(3)	O7-Cu-H ₂ O1	82.9(3)
O7-Cd-O6	96.0(3)	O5-Cu-H ₂ O1	90.7(3)
O4-Cd-O6	85.3(3)	O6-Cu-H ₂ O1	166.4(3)
O3-Cd-H ₂ O2	91.0(3)	O7-Cu-H ₂ O2	102.6(3)
O7-Cd-H ₂ O2	145.3(2)	O5-Cu-H ₂ O2	93.6(3)
O4-Cd-H ₂ O2	80.8(3)	O6-Cu-H ₂ O2	81.9(3)
O6-Cd-H ₂ O2	76.0(2)	H ₂ O1-Cu-H ₂ O2	85.0(3)
O3-Cd-H ₂ O1	94.6(3)	O1-S-O2	109.8(7)
O7-Cd-H ₂ O1	66.3(2)	O1-S-O3	109.0(5)
O4-Cd-H ₂ O1	156.6(3)	O2-S-O3 ×2	110.7(4)
O6-Cd-H ₂ O1	78.5(2)	O1-S-O3	109.0(5)
H ₂ O2-Cd-H ₂ O1	79.0(2)	O3-S-O3	107.7(8)
O4-P-O5	114.4(4)		
O4-P-O6	109.6(4)		
O5-P-O6	110.0(4)		
O4-P-O7	111.4(4)		
O5-P-O7	102.4(4)		
O6-P-O7	108.8(4)		
Atomic separations corresponding to possible hydrogen bonds			
H ₂ O1 ×2...O1	2.888	H ₂ O2 ×2...H ₂ O3	2.673
H ₂ O1...O4	2.606	H ₂ O3...O3 ×2	2.959
H ₂ O2...O2	2.829	H ₂ O3...O2	2.673
H ₂ O2 ×2...O1	3.127	H ₂ O3...H ₂ O2 ×2	2.673

The (Cdφ₆) octahedron shares an edge with the (Cuφ₅) square-pyramid. The mean edge length of the (Cuφ₅) square-pyramid (3.00 Å) is considerably less than that of the (Cdφ₆) octahedron (3.22 Å). As they have a common edge, across which cation-cation repulsion occurs, the polyhedra must distort from their holosymmetric configurations.

The structure contains one P site that is completely occupied by P and coordinated by four O atoms in a tetrahedral arrange-

TABLE 6. Bond-valence analysis for birchite

	Cu	Cd	P	S	H1	H2	H3	H4	H5	H6	Sum (excluding H)	Sum (including H)
O1				1.57	0.15 ×2		0.04 ×2				1.57	1.95
O2				1.50			0.16		0.21		1.50	1.87
O3		0.43		1.44 ↓→ 1.44 ↓					0.12		1.87	1.99
O4		0.40	1.32			0.23					1.72	1.95
O5	0.54		1.27								1.81	1.81
O6	0.46	0.38	1.20								2.04	2.04
O7	0.53	0.41	1.16								2.09	2.09
H ₂ O1	0.36	0.17			0.70	0.77					0.54	2.01
H ₂ O2	0.16	0.29					0.76	0.58		0.21	0.45	2.00
H ₂ O3								0.21 ×2	0.67	0.79	0	1.89
Sum	2.05	2.08	4.95	5.95	1.00	1.00	1.00	1.00	1.00	1.00		

**FIGURE 5.** Coordination around the Cd site in birchite, showing the short Cd-O5 distance.

ment, with a $\langle\text{P-O}\rangle$ distance of 1.538 Å (range: 1.515–1.562 Å) (Table 5), which is in accord with the average $\langle\text{P-O}\rangle$ distance of 1.537 Å (range: 1.439–1.625 Å) for phosphate minerals (Baur 1981; Huminicki and Hawthorne 2002). Bond-valence calculations (Table 6) and bond lengths strongly indicate complete occupancy of the site by P.

The structure contains one S site, which lies on a mirror plane, coordinated by four O atoms in a tetrahedral arrangement, with a $\langle\text{S-O}\rangle$ distance of 1.476 Å (range: 1.456–1.488 Å), which is in agreement with the average $\langle\text{S-O}\rangle$ length of 1.473 Å typical for a sulfate ion (Baur 1972). Bond-valence calculations (Table 6) and bond lengths (Table 5) are in accord with complete occupancy of the site by S.

Anion sites

There are 10 anion sites in the structure, each occupied by O atoms. The bond-valence sums for the O atoms of the H₂O1 (0.55 valence units, v.u.), and H₂O2 (0.45 v.u.) sites (Table 6), clearly indicate the presence of (H₂O) groups. The H₂O1 and H₂O2 sites link to both the Cu and Cd sites. The bond-valence sum for the O atom of the H₂O3 site, (0.0 v.u.), indicates the presence of an interstitial water molecule not bonded to any of the cations, and held in the structure by hydrogen bonds only.

Structure topology

The {CdO₄(H₂O)₂} octahedra are linked by edge-sharing to the {CuO₃(H₂O)₂} square-pyramids forming infinite chains, of composition [Cd,Cu(H₂O)₂O₅], and with a staggered geometry, that extend along the *a* direction. Each chain is decorated with (PO₄) tetrahedra to form a [Cd,Cu(PO₄)(H₂O)₂O₄] chain. The chains are cross-linked in the *b* direction by sharing both octahedra and square-pyramid vertices with vertices of (PO₄) tetrahedra, to form sheets of composition [CdCu(PO₄)(H₂O)₂O] in the (010) plane (Fig. 6). Two sheets, which are symmetrically related by a screw dyad, are linked by (PO₄) tetrahedra vertices to form a layer in the (010) plane. Two layers, which are related by mirror symmetry, are linked by (SO₄) tetrahedra via corner-sharing with {CdO₄(H₂O)₂} octahedra to form a heteropolyhedral framework structure (Fig. 7).

Interstitial channels within the framework extend along both the *a* and *c* directions and are occupied by the water molecule H₂O3 and the hydrogen atoms of the H₂O1 and H₂O2 groups that coordinate to the Cd and Cu cations.

Hydrogen-bonding

Using stereochemical considerations and bond-valence calculations (Table 6) a probable hydrogen-bond system was derived (Brown and Altermatt 1985; Brese and O'Keeffe 1991; Brown 1996). Without considering the contributions of hydrogen atoms, the bond strengths reaching the oxygen atoms of (H₂O) groups H₂O1, H₂O2, and H₂O3 are 0.55, 0.46, and 0.0 v.u., respectively, indicating their probable role as providers of hydrogen bonds. O atoms O1, O2, O3, and O4 with bond strengths of 1.58, 1.55, 1.89, and 1.75 v.u., respectively, are undersaturated. Therefore, based on the dependence of H-O bond-valence on O...O distance (Table 5), they are likely acceptors of hydrogen bonds, which provide the necessary increase of their respective bond-valence.

The hydrogen bonds donated by the H₂O1 group are likely accepted by O1 and O4. Thus the H₂O1 group is in an approximately tetrahedral coordination as is common for H₂O groups in mineral structures (Hawthorne 1992), with bonds to the Cu²⁺ and Cd²⁺ cations and the donation of two hydrogen bonds.

The H₂O2 group likely donates a hydrogen bond that is accepted by H₂O3, and also a bifurcated hydrogen bond accepted by O2 and O1. The H₂O2 group also accepts a hydrogen bond from the H₂O3 group.

The H₂O3 group likely donates a trifurcated hydrogen bond that is accepted by two O3 atoms in adjacent positions of a (SO₄) tetrahedron and by an O2 atom on an adjacent SO₄ tetrahedron, and also donates a bifurcated hydrogen bond that is accepted by

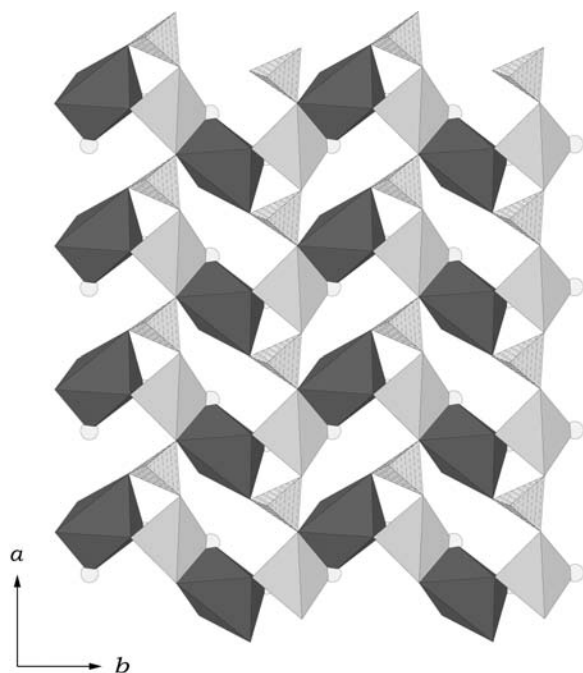


FIGURE 6. The crystal structure of birchite projected onto (010) showing $[\text{Cd,Cu}(\text{H}_2\text{O})_2\text{O}_5]$ chains extending along the a axis, and linked by (PO_4) tetrahedra to form a $[\text{Cd,Cu}(\text{PO}_4)(\text{H}_2\text{O})_2\text{O}_4]$ sheet. $(\text{Cu}\phi_5)$ square-pyramids = light gray; $(\text{Cd}\phi_6)$ octahedral = dark gray; PO_4 tetrahedra = dash-shaded; SO_4 tetrahedra = cross-shaded. Water molecules = pale gray circles.

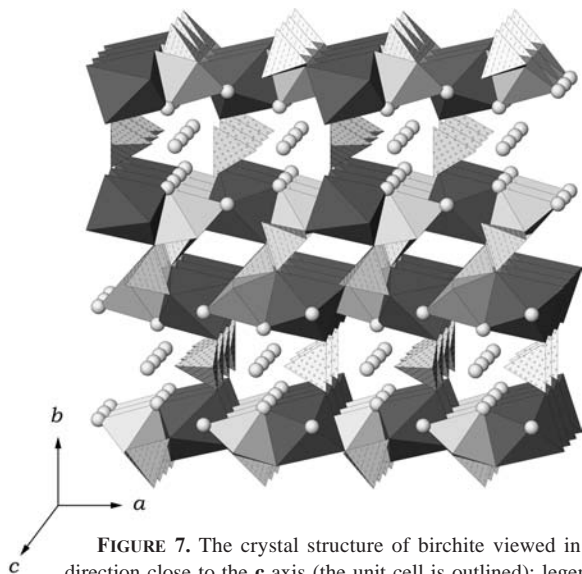


FIGURE 7. The crystal structure of birchite viewed in a direction close to the c axis (the unit cell is outlined); legend as in Figure 6.

two H_2O_2 groups in adjacent layers of the structure. The H_2O_3 group likely accepts hydrogen bonds from two H_2O_2 groups in adjacent layers of the structure.

The suggested hydrogen bonds would represent medium-weak links, as the $\text{O}\cdots\text{O}$ distances range from 2.67(3) to 3.12(7) Å. These bonds provide additional linkage between the sheets in the structure via the involved polyhedra.

RELATED STRUCTURES

To the authors' best knowledge, no compounds with closely related structures have been reported in the literature. Eby and Hawthorne (1993) have noted that of the fivefold-coordinated Cu^{2+} polyhedra, the square-pyramid is much more common than the trigonal-bipyramid, which occurs in only a small number of mineral structures. Most mineral structures that contain $(\text{Cu}\phi_5)$ square-pyramids also contain $(\text{Cu}\phi_6)$ octahedra; only ziesite, blossite, kinoite, and juabite contain Cu^{2+} that is only present in the square-pyramidal coordination (Burns et al. 2000).

Of the previously reported oxysalt minerals with fivefold-coordinated Cu^{2+} (Eby and Hawthorne 1993), none share the motif of $[\text{M}_2\phi_n]$ chains, composed of edge-sharing $(\text{Cu}\phi_5)$ polyhedra and $(\text{M}\phi_6)$ octahedra. The $(\text{Cu}\phi_5)$ square-pyramid in structures usually shares an edge with another square-pyramid to form a $[\text{Cu}_2\phi_8]$ dimer. Examples include the structures of ziesite (Mercurio-Lavaud and Frit 1973) and blossite (Calvo and Faggiani 1975). The structure of kinoite contains chains of edge-sharing $(\text{Cu}\phi_5)$ square-pyramids (Laughton 1971). The main motif in the structure of leogangite comprises four $(\text{Cu}\phi_5)$ square-pyramids joined to form a $[\text{Cu}_4\text{O}_{14}]$ tetramer, which links to two corners of an (AsO_4) tetrahedron, and to a (CuO_5) distorted trigonal bipyramid, to form a complex heteropolyhedral layer (Lengauer et al. 2004). The layers link via (SO_4) tetrahedra to form an open framework structure.

Of the Cu minerals with both fivefold- and sixfold-coordinated cations, the structure of jubaitite contains chains composed of edge-sharing $(\text{Cu}\phi_5)$ square-pyramids, forming $[\text{Cu}_2\phi_8]$ dimers, which link by edge-sharing to (CaO_6) octahedra (Burns et al. 2000). The stranskiite structure comprises staggered $[\text{M}_2\phi_n]$ chains of $\text{Cu}^{[4+2]}$ tetragonal dipyramids and dimers of edge-sharing $\text{Zn}^{[3+2]}$ trigonal dipyramids linked into a framework by (AsO_4) tetrahedra (Keller et al. 1979).

ACKNOWLEDGMENTS

The authors thank Angus Netting of Adelaide Microscopy, The University of Adelaide for assistance in obtaining the electron-microprobe analysis and Bill Aird for assistance with the SEM photomicrographs.

REFERENCES CITED

- Baur, W.H. (1972) Prediction of hydrogen-bonds and hydrogen atom positions in crystalline solids. *Acta Crystallographica*, B28, 1456–1465.
- (1981) Interatomic distance predictions for computer simulation of crystal structures. In M. O'Keeffe and A. Navrotsky, Eds., *Structure and Bonding in Crystals II*, p. 31–52. Academic Press, New York.
- Birch, W.D. (1990) Minerals from the Kintore and Block 14 Opencuts, Broken Hill, New South Wales: A review of recent discoveries, including tsumebite, kipushite, and otavite. *Australian Mineralogist*, 5, 125–141.
- (1999) The Minerals. In W.D. Birch, Ed., *Minerals of Broken Hill*, p. 88–256. Broken Hill Council, New South Wales.
- Birch, W.D. and van der Heyden, A. (1988) Minerals of the Kintore Opencut, Broken Hill, New South Wales. *Mineralogical Record*, 19, 425–436.
- (1997) Minerals from the Kintore and Block 14 Open cuts, Broken Hill, New South Wales. *Australian Journal of Mineralogy*, 3, 23–71.
- Birch, W.D., Chapman, A., and Peacock, S.R. (1982) The minerals. In H.K. Wörner and R. Mitchell, Eds., *Minerals of Broken Hill*, p. 68–185. Australian Mining and Smelting Limited, Melbourne.
- Birch, W.D., Pring, A., and Gatehouse, B.M. (1992) Segnitite $\text{PbFe}_2\text{H}(\text{AsO}_4)_2(\text{OH})_6$, a new mineral in the lusungite group from Broken Hill, New South Wales, Australia. *American Mineralogist*, 77, 656–659.
- Brese, N.E. and O'Keeffe, M. (1991) Bond-valence parameters for solids. *Acta Crystallographica*, B47, 192–197.
- Brown, I.D. (1996) VALENCE: a program for calculating bond-valences. *Journal of Applied Crystallography*, 29, 479–480.
- Brown, I.D. and Altermatt, D. (1985) Bond-valence parameters obtained from a

- systematic analysis of the inorganic crystal structure database. *Acta Crystallographica*, B41, 244–247.
- Burns, P.C. and Hawthorne, F.C. (1995) Coordination-geometry structural pathways in Cu^{2+} oxysalt minerals. *Canadian Mineralogist*, 33, 889–905.
- Burns, P.C., Clark, C.M., and Gault, R.A. (2000) Juabite, $\text{CaCu}_{10}(\text{Te}^{4+}\text{O}_3)_4(\text{AsO}_4)_4(\text{OH})_2(\text{H}_2\text{O})_4$: Crystal structure and revision of chemical formula. *Canadian Mineralogist*, 38, 809–816.
- Calvo, C. and Faggiani, R. (1975) α Cupric divanadate. *Acta Crystallographica*, B31, 603–605.
- Cooper, M.A. and Hawthorne, F.C. (1996) The crystal structure of keyite, $\text{Cu}_3(\text{Zn,Cu})_6\text{Cd}_2(\text{AsO}_4)_6(\text{H}_2\text{O})_2$, an oxysalt mineral with essential cadmium. *Canadian Mineralogist*, 34, 623–630.
- (2000) Highly undersaturated anions in the crystal structure of andyrobite-calcio-andyrobite, a doubly acid arsenate of the form $\text{K}(\text{Cd,Ca})[\text{Cu}_2^+(\text{AsO}_4)_4\{\text{As}(\text{OH})_2\text{O}_2\}](\text{H}_2\text{O})_2$. *Canadian Mineralogist*, 38, 817–830.
- (2004) The crystal structure of goldquarryite, $(\text{Cu}^{2+}\square)(\text{Cd,Ca})_2\text{Al}_3(\text{PO}_4)_4\text{F}_2(\text{H}_2\text{O})_{10}(\text{H}_2\text{O},\text{F})_2$, a secondary phosphate from the Gold Quarry mine, Eureka County, Nevada, U.S.A. *Canadian Mineralogist*, 42, 753–761.
- Coppens, P. (1970) *Crystallographic Computing*; F.R. Ahmed, S.R. Hall, and C.P. Huber, Eds., p. 255–270. Munksgaard, Copenhagen.
- Eby, R.K. and Hawthorne, F.C. (1990) Clinoclase and the geometry of [5]-coordinate Cu^{2+} in minerals. *Acta Crystallographica*, C46, 2291–2294.
- (1993) Structural relations in copper oxysalt minerals. I. Structural hierarchy. *Acta Crystallographica*, B49, 28–56.
- Edwards, A.B. (1955) Cadmium in the Broken Hill lode. *Proceedings of the Australasian Institute of Mining and Metallurgy*, 176, 71–96.
- Effenberger, H. (1988) Contribution to the stereochemistry of copper. The transition from a tetragonal pyramidal to a trigonal bipyramidal $\text{Cu}(\text{II})\text{O}_5$ coordination figure with a structure determination of $\text{PbCu}_2(\text{SeO}_3)_3$. *Journal of Solid State Chemistry*, 73, 118–126.
- Giester, G., Rieck, B., and Brandstätter, F. (1998) Niedermayrite, $\text{Cu}_4\text{Cd}(\text{SO}_4)_2(\text{OH})_6\cdot 4\text{H}_2\text{O}$, a new mineral from the Lavrion District, Greece. *Mineralogy and Petrology*, 63, 9–34.
- Giester, G., Kolitsch, U., Leverett, P., Turner, P., and Williams, P.A. (2007) The crystal structures of lavendulan, sampleite, and a new polymorph of sampleite. *European Journal of Mineralogy*, 19, 75–93.
- Hawthorne, F.C. (1992) The role of OH and H_2O in oxide and oxysalt minerals. *Zeitschrift für Kristallographie*, 201, 183–206.
- Huminicki, D.M.C. and Hawthorne, F.C. (2002) The crystal chemistry of the phosphate minerals. In M.J. Kohn, J. Rakovan, and J.M. Hughes, Eds., *Phosphates: Geochemical, Geobiological, and Materials Importance*, 48, p. 123–253. *Reviews in Mineralogy and Geochemistry*, Mineralogical Society of America, Chantilly, Virginia.
- Keller, P., Hess, H., and Dunn, P.J. (1979) Die Ladungsbilanz für eine verfeinerte Kristallstruktur von Stranskiit, $\text{Zn}_2\text{Cu}(\text{AsO}_4)_2$. *Tschermaks Mineralogische und Petrographische Mitteilungen*, 26, 167–174.
- Laughon, R.B. (1971) The crystal structure of kinoite. *American Mineralogist*, 56, 193–200.
- Le Bail, A., Duroy, H., and Fourquet, J.L. (1988) Ab-initio structure determination of LiSbWO_6 by X-ray powder diffraction. *Materials Research Bulletin*, 23, 447–452.
- Lengauer, C.L., Giester, G., and Kirchner, E. (2004) Leogangite, $\text{Cu}_{10}(\text{AsO}_4)_4(\text{SO}_4)(\text{OH})_6\cdot 8\text{H}_2\text{O}$, a new mineral from the Leogang mining district, Salzburg province, Austria. *Mineralogy and Petrology*, 81, 187–201.
- Mandarino, J.A. (1981) The Gladstone-Dale relationship: Part IV: The compatibility concept and its application. *Canadian Mineralogist*, 19, 441–450.
- Mercurio-Lavaud, D. and Frit, B. (1973) Structure cristalline de la variété basse température du pyrovanadate de cuivre: $\text{Cu}_2\text{V}_2\text{O}_7\alpha$. *Acta Crystallographica*, B29, 2737–2741.
- Nriagu, J.O. (1984) Formation and Stability of Base Metal Phosphates in Soils and Sediments. In J.O. Nriagu and P.B. Moore, Eds., *Phosphate Minerals*, p. 292–317. Springer, Berlin.
- Otwinowski, Z., Borek, D., Majewski, W., and Minor, W. (2003) Multiparametric scaling of diffraction intensities. *Acta Crystallographica*, A59, 228–234.
- Plimer, I.R. (1984) The mineralogical history of the Broken Hill Lode, NSW. *Australian Journal of Earth Sciences*, 31, 379–402.
- Pouchou, J.L. and Pichoir, F. (1985) “PAP” $\phi(\rho Z)$ procedure for improved quantitative microanalysis. *Microbeam Analysis*, 104–106.
- Pring, A., McBriar, E.M., and Birch, W.D. (1989) Mawbyite, a new arsenate of lead and iron related to tsumcorite and carminite, from Broken Hill, New South Wales. *American Mineralogist*, 74, 1377–1381.
- Pring, A., Birch, W.D., Dawe, J.R., Taylor, M.R., Deliens, M., and Walenta, K. (1995) Kintoreite, $\text{PbFe}_3(\text{PO}_4)_2(\text{OH},\text{H}_2\text{O})_6$, a new mineral of the jarosite-alunite family, and lusungite discredited. *Mineralogical Magazine*, 59, 143–148.
- Roberts, A.C., Cooper, M.A., Hawthorne, F.C., Jensen, M.C., and Foord, E.E. (2003) Goldquarryite, a new Cd-bearing phosphate mineral from the Gold Quarry Mine, Eureka County, Nevada. *Mineralogical Record*, 34, 237–240.
- Shape Software (1997) *ATOMS for Windows and Macintosh V 4.0*. Kingsport, Tennessee.
- (2004) *SHAPE for Windows and Macintosh V 7.1.2*. Kingsport, Tennessee.
- Sheldrick, G.M. (1997a) *SHELXS-97, a Program for the Solution of Crystal Structures*. University of Göttingen, Göttingen, Germany.
- (1997b) *SHELXL-97, a Program for Crystal Structure Refinement*. University of Göttingen, Göttingen, Germany.
- Stanton, R.L. (1976) *Petrochemical Studies on the Chemical Metasediments of the Broken Hill Ore Environment*. Institution of Mining and Metallurgy, Transactions Section B, B221–223.
- Wavemetrics, Inc. (2000) *IGOR PRO version 4.0*. WaveMetrics Inc., Lake Oswego, Oregon.
- Williams, P.A. (1990) *Oxide Zone Geochemistry*, 286p. Ellis Horwood, New York.
- Wilson, A.I.C. (1992) *International tables for crystallography*, vol. C, 883 p. Kluwer Academic, Dordrecht, The Netherlands.
- Yvon, K., Jeitschko, W., and Parthe, E. (1977) *LAZY PULVERIX*, a computer program, for calculating X-ray and neutron diffraction powder patterns. *Journal of Applied Crystallography*, 10, 73–74.

MANUSCRIPT RECEIVED JULY 5, 2007

MANUSCRIPT ACCEPTED DECEMBER 26, 2007

MANUSCRIPT HANDLED BY PAOLA BONAZZI